NANO · MICRO small
www.small-journal.com

H_2S-Scavenged and Activated Iron Oxide-Hydroxide Nanospindles for MRI-Guided Photothermal Therapy and Ferroptosis in Colon Cancer

Yangyang Li, Weiyu Chen, Yuchen Qi, Shuai Wang, Lei Li, Wanlin Li, Tingting Xie, Huanle Zhu, Zhe Tang,* and Min Zhou**

Overproduced hydrogen sulfide (H_2S) is of vital importance for the progress of colon cancer and promotes cancer cellular proliferation. Devising pharmacological nanomaterials for tumor-specific H_2S activation will be significant for precise colon cancer treatment. Herein, a biocompatible fusiform iron oxide-hydroxide nanospindles (FeOOH NSs) nanosystem for magnetic resonance imaging (MRI), ferroptosis, and H_2S based cascade reaction-enhanced combinational colon cancer treatment is developed. The FeOOH NSs can effectively scavenge endogenous H_2S via the reduction reaction to prohibit the growth of CT26 colon cancer. The cascade produced FeS driven by overexpressed H_2S exhibits near-infrared-triggered photothermal therapy capability and Fe^{2+}-mediated ferroptosis functionality. Meanwhile, the as-prepared FeOOH NSs can light up tumor tissues as a potent MRI contrast agent. Additionally, FeOOH NSs present desirable biosafety in a murine model for up to three months and avoid any long-term toxicity. Furthermore, it is found that these H_2S-responsible nanotheranostics do not cause any cure effects on other cancer types, such as 4T1 breast cancer. Overall, the findings illustrate that the biocompatible FeOOH NSs can be successfully employed as a theranostic for specifically treating colon cancer, which may promote the clinical translation and development of H_2S-responsive nanoplatforms.

1. Introduction

Colon cancer is one of the most common cancers globally, with a high level of mortality.[1] As the general clinical strategies, surgical resection, radiotherapy, and chemotherapy have been widely applied in treating colorectal cancer.[2] However, those therapeutic approaches, especially radiotherapy and chemotherapy, are always accompanied by various side effects, for instance, fatigue and appetite.[3] More importantly, the heterogeneous cancer cells might become resistant to the chemotherapy applied, eventually leading to the recurrence and metastasis of tumors.[4] Additionally, the surgical procedures have to suffer from the recurrence, metastasis, and great pain to patients.[5] Hence, an effective agent for colon cancer theranostic is highly demanded.

As one major gasotransmitter, endogenous hydrogen sulfide (H_2S) is of vital importance in various physical and biological functions, which is strongly associated

Dr. Y. Y. Li, Y. C. Qi, S. Wang, Prof. Z. Tang, Prof. M. Zhou
Department of Surgery
The Fourth Affiliated Hospital
Zhejiang University School of Medicine
Yiwu 322000, China
E-mail: 8xi@zju.edu.cn; zhoum@zju.edu.cn

Dr. W. Y. Chen
Molecular Imaging Program at Stanford
Department of Radiology
Stanford University
Stanford, CA 94305-5427, USA

Dr. L. Li
Shanghai Key Laboratory of Regulatory Biology
Institute of Biomedical Sciences
School of Life Sciences
East China Normal University
Shanghai 200241, China
E-mail: lli@bio.ecnu.edu.cn

The ORCID identification number(s) for the author(s) of this article can be found under https://doi.org/10.1002/smll.202001356.

W. L. Li, T. T. Xie, Prof. M. Zhou
Institute of Translational Medicine
Zhejiang University
Hangzhou 310009, China

H. L. Zhu
Department of Radiology
Sir Run Run Shaw Hospital
Zhejiang University School of Medicine
Hangzhou, Zhejiang 310016, China

Prof. M. Zhou
State Key Laboratory of Modern Optical Instrumentations
Zhejiang University
Hangzhou 310058, China

DOI: 10.1002/smll.202001356

with a series of diseases, such as cancer.[6,8] Notably, a great amount of H_2S was produced within colon cancer cells due to the overexpression of cystathionine-β-synthase (CBS), one type of H_2S producing enzyme. The produced endogenous H_2S can promote colon cancer cell proliferation and angiogenesis around the tumors tissue.[7] Pharmacological inhibition or blocking of CBS expression has been proved to reduce the tumor functions in terms of bioenergetics, angiogenesis, and growth caused by produced H_2S.[1a,7a,8] However, efficient scavenge of endogenous H_2S may be another promising approach for colorectal tumor growth inhibition.

As promising candidates, multifunctionalized nanomaterials demonstrate great potential in cancer detection and therapy. Although various nanomaterials have been employed in fighting colon cancer via the H_2S-triggered detection and treatment,[9] raw was designed for scavenging H_2S simultaneously.[10] Previously, paramagnetic iron oxide-hydroxide (FeOOH) nanospindles (NSs) have been successfully utilized as a magnetic resonance imaging (MRI) contrast agent for cancer diagnosis.[11] More importantly, the FeOOH NSs have also been employed for sensing and removing H_2S gas, showing a high reactivity and adsorption capacity of hydrogen sulfide under room temperature and ambient pressure.[12] Therefore, the FeOOH NSs with MRI and H_2S scavenging properties hold great prospects in colon cancer theranostics.

Notably, photothermal therapy (PTT) has been widely applied as a therapeutic module in various imaging-guided (ranging from MRI to photoacoustic imaging) cancer therapy.[13] Up to now, a variety of near-infrared (NIR) irradiated PTT agents including gold nanoparticles, metal sulfide material, and organic dyes, have been successfully employed in tumor theranostics.[14] Nevertheless, these traditional PTT nanoplatforms could not completely prevent the mis-targeting effects during the PTT process, which would cause severe damage to normal tissues. Recently, several H_2S-activated photothermal agents have been applied in treating colorectal cancer.[10,15] Particularly, inorganic Cu_2O based nanoparticles could be sulfidated as Cu_9S_8 within the colorectal tumors, presenting the photothermal capability with NIR irradiation.[16] However, the performance of H_2S removal has not been investigated and the potential toxicity caused by Cu element could not be easily ignored.[17] In comparison, the sulfidated product of FeOOH NSs, FeS exhibited not only high biocompatibility but also presented desirable MRI and PTT functions for treating cancer.[18] More importantly, the iron element based nanoparticle is able to induce the death of cancer cells via the ferroptosis as well.[19] All these illustrate the great potential of FeOOH NSs as a smart nanoagent in colorectal cancer theranostics.

Herein, we designed a FeOOH NSs nanosystem to image and treat colorectal tumors using their H_2S-scavenged property, cascade produced FeS with photothermal therapy capability, and ferroptosis functionality. FeOOH NSs could efficiently adsorb the endogenous H_2S of the CT26 colon tumor and thus inhibit its growth. The specifically generated photothermal FeS was able to further kill the cancer cells via NIR laser irradiation. We also found that the FeS demonstrated ferroptosis to colon cancer. Moreover, these FeOOH NSs were able to light up the tumor via MRI function and performed image-guided tumor therapy. Current findings clearly demonstrate that these MRI-guided and H_2S-responsive FeOOH NSs could be applied in precision colon cancer theranostic. And this novel design may inspire and promote the development of smart nanomedicine for colon cancer therapy in responding to endogenous H_2S.

2. Results and Discussion

2.1. Physiochemical Features of Mesoporous FeOOH Nanospindles

As-prepared FeOOH NSs presented a uniform spindle shape with the size around 10×40 nm under transmission electron microscopy (TEM) imaging (**Figure 1**a), which is consistent with the hydrodynamic diameter (≈50 nm) (Figure 1d). The energy dispersive X-ray spectroscopy (EDS) and high-resolution TEM (HRTEM) images clearly clarify the homogeneous crystal structure of FeOOH NSs by showing the well-distributed elements and the identical atomic arrangement with an interlay spacing at 0.255 nm (Figure 1b,c). Consistent with the previous study, typical peaks including 110, 200, 220, and 221 were observed in X-ray diffraction (XRD) patterns, further confirming the crystal structure of FeOOH NSs (Figure 1e).[21] Since now, polymers such as polyethylene glycol (PEG) have been widely employed as surface functional groups to enhance the circulation of nanomaterials.[22] To promote the stability of FeOOH nanospindles, FeOOH NSs were further functionalized with PEG that slightly increased the diameter of NSs (≈80 nm) (Figure S1a, Supporting Information). The X-ray photoelectron spectroscopy (XPS) patterns and decreased zeta potential further verified the modification of polyethylene glycol on FeOOH NSs (Figure S1b–d, Supporting Information). Moreover, TEM images of PEG-modified FeOOH revealed an amorphous polymer shell covering the surface. Further, the EDS spectrum demonstrated the existence of Fe, O, N, and C elements in the PEG-modified FeOOH, suggesting the successful PEG-NH_2 molecules modification of FeOOH (Figure S2, Supporting Information). The PEGylation well stabilized the FeOOH NSs by preventing any significant aggregation and precipitation in various media (H_2O, phosphate buffered saline (PBS), and Dulbecco's modified Eagle's medium (DMEM)) up to 5 d (Figure S3b,c, Supporting Information). More importantly, the obtained PEGylation FeOOH (abbreviated as FeOOH NSs) still presented a large surface area of 89.7 $m^2\ g^{-1}$ and a pore volume of 0.374 $cm^2\ g^{-1}$, with average pore size at ≈4.5 nm (Figure 1f,g and Figure S3a, Supporting Information). In consideration of the acidic environment in tumor microenvironment (TME), the stability of FeOOH NSs in response to pH was further investigated. Notable, as a weak base, FeOOH NSs quickly dissolved and neutralized acidic buffer (pH = 5.0 or 6.0) to around pH = 6.5, while it was stable within the neutral environment (Figure 1h). As the pH values were about 6.5–6.9 within TME, this spindle-shaped nanoagent would remain intact when they accumulated in the tumor area. Therefore, the large surface area and pore volume could be well maintained for the interaction and adsorption of H_2S.

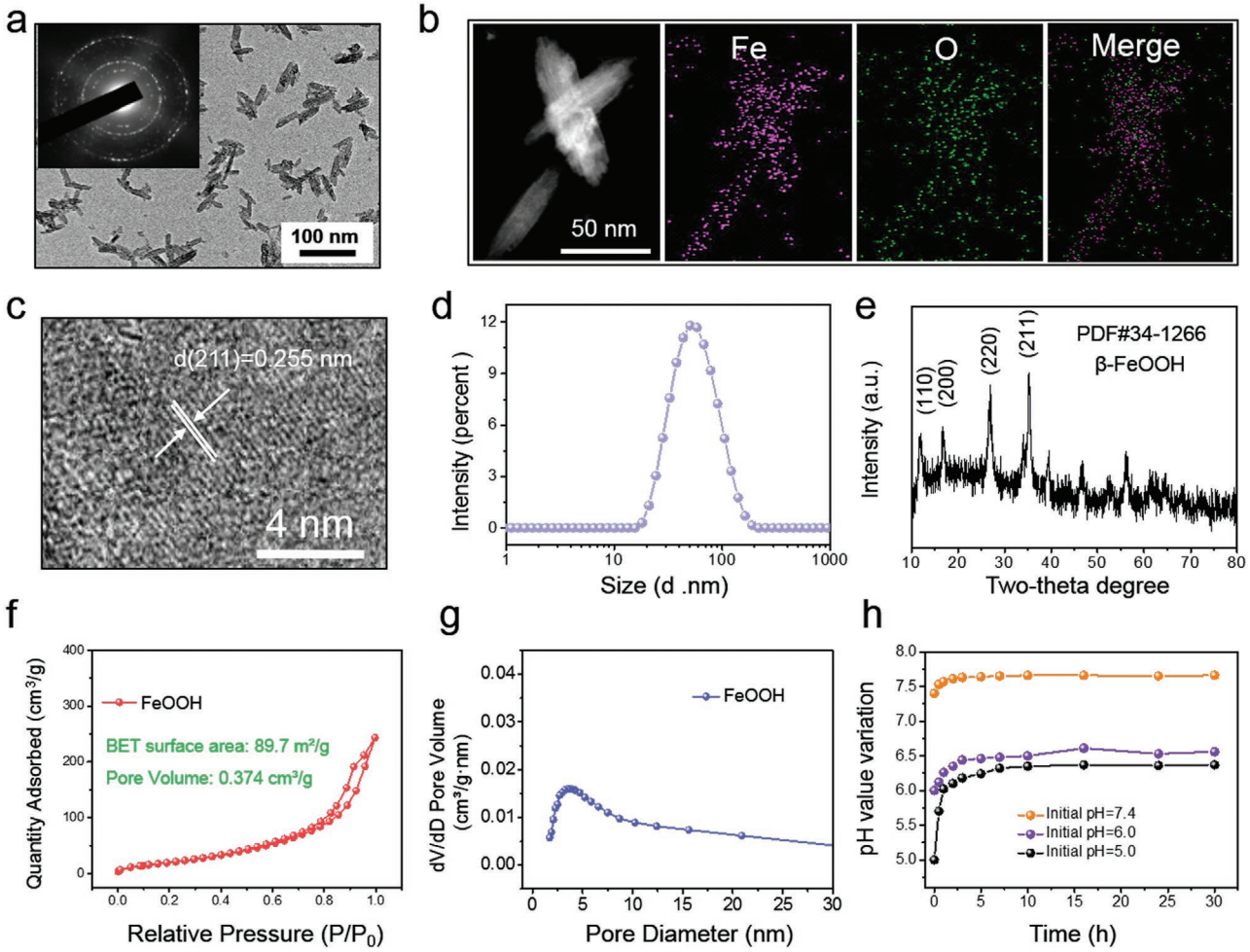

Figure 1. Synthesis and characterization of mesoporous FeOOH nanospindles (NSs). a) TEM images and b) elemental mapping patterns of FeOOH NSs. The inset image shows the corresponding selected area electron diffraction pattern. c) The HRTEM image of crystalline FeOOH NSs. d) Dynamic light scattering data of FeOOH NSs in aqueous solution. e) XRD pattern of FeOOH NSs. f) N_2 adsorption/desorption isotherm of the PEG-modified FeOOH NSs (abbreviated as FeOOH NSs). g) The pore size distribution of modified FeOOH NSs in N_2 adsorption/desorption isotherm. h) The pH changes of different solutions (pH = 5.0, 6.0, or 7.4) after the addition of the modified FeOOH NSs.

2.2. The H_2S-Activated Photothermal Capability of FeOOH NSs

As one of metal sulfide nanomaterials, FeS nanoparticles have been developed as photothermal agents for tumor therapy via NIR irradiation.[18] Given that the FeS could be smartly generated after the interaction between as-designed FeOOH NSs and hydrogen sulfide, the H_2S-triggered photothermal capability was comprehensively examined. With the presentation of NaHS, FeOOH NSs could quickly interact and absorb H_2S by generating the FeS component (**Figure 2**a and Figure S4, Supporting Information). As can be seen in TEM and related EDS spectrum and element mapping, small and intensive FeS nanospindles emerged on the surface of FeOOH nanomaterial after the NaHS exposure, with the diameter around 5 nm (Figure 2b–d). The elemental mapping patterns (Figure S4, Supporting Information) and the EDS spectrum (Figure 2d) both demonstrated the existence of Fe, O, and S elements. In contrast, S element did not exist until the reaction with NaHS as demonstrated in Figure 1b,d. These FeS nanoparticles brought a sharp NIR absorption peak at 660 nm, lighting up the PTT capability of FeOOH NSs (Figure 2e). It can be clearly seen that the efficiency of PTT is linearly related to the concentration of iron nanospindles and the powder of laser with the attendance of NaHS (Figure 2f–i). Specifically, the FeS and FeOOH-PEG NSs could rapidly increase the temperature to 50 °C after 100 s irradiation, eventually reaching 60 °C within 5 min (Figure 2g,i). As the necroptosis and apoptosis of cancer cells could be achieved by PTT when the temperature is higher than 46 °C, the PTT mediated by FeOOH NSs would be fully effective to ablate tumors.[23] More importantly, the photothermal function of FeOOH NSs was totally muted when the NaHS was absent (Figure S5, Supporting Information). Since now, various nanomaterials have been applied in tumor photothermal therapy, but most agents present PTT function constantly,[14a] which would potentially increase damage on normal tissue via off-target nanospindles. Comparably, these smart nanoparticles could efficiently avoid this side effect and only generate PTT within the tumor area, providing a precision therapy for colon cancer.

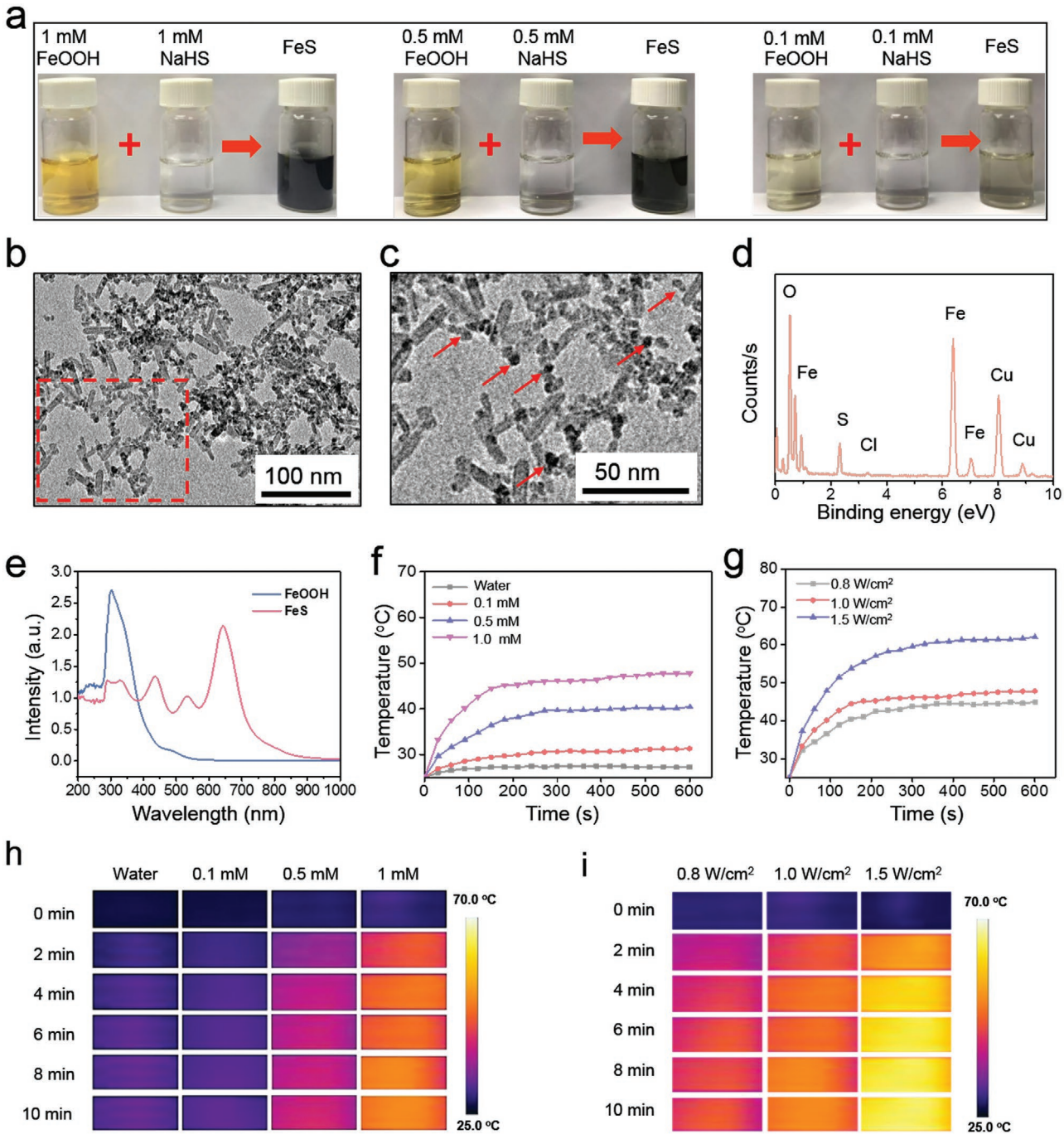

Figure 2. Characterization of FeOOH NSs in the aqueous dispersion and the performance in the presence of NaHS. a) A photograph of FeOOH NSs at different concentrations in the presence of NaHS. b–d) TEM, magnified TEM images, and energy dispersive X-ray spectroscopy (EDX) of the FeOOH NSs after the addition of NaHS solution. The arrows indicate the generated FeS. e) Ultraviolet–visible absorption spectroscopy of FeOOH NSs and FeS. f,h) Representative temperature variation curves and corresponding thermal images of the aqueous dispersion of FeOOH NSs at various concentrations (0.1, 0.5, and 1×10^{-3} M) with the attendance of NaHS under 808 nm laser irradiation at 1.0 W cm^{-2}. g,i) Representative temperature variation curves and corresponding thermal images of FeOOH NSs (1×10^{-3} M) in the presence of NaHS under 808 nm laser irradiation with different power densities (0.8, 1.0, and 1.5 W cm^{-2}).

2.3. Selective Cytotoxicity of FeOOH NSs

Efficient cellular uptake of therapeutic nanoparticles into cancer cells is vital for drug delivery. The FeOOH were labeled with IR780 (FOOH/IR780) fluorescent molecules to investigate the cellular uptake performance by measuring IR780 characteristic red fluorescence by using a confocal laser scanning microscope (CLSM). The CLSM images demonstrated that most of the red

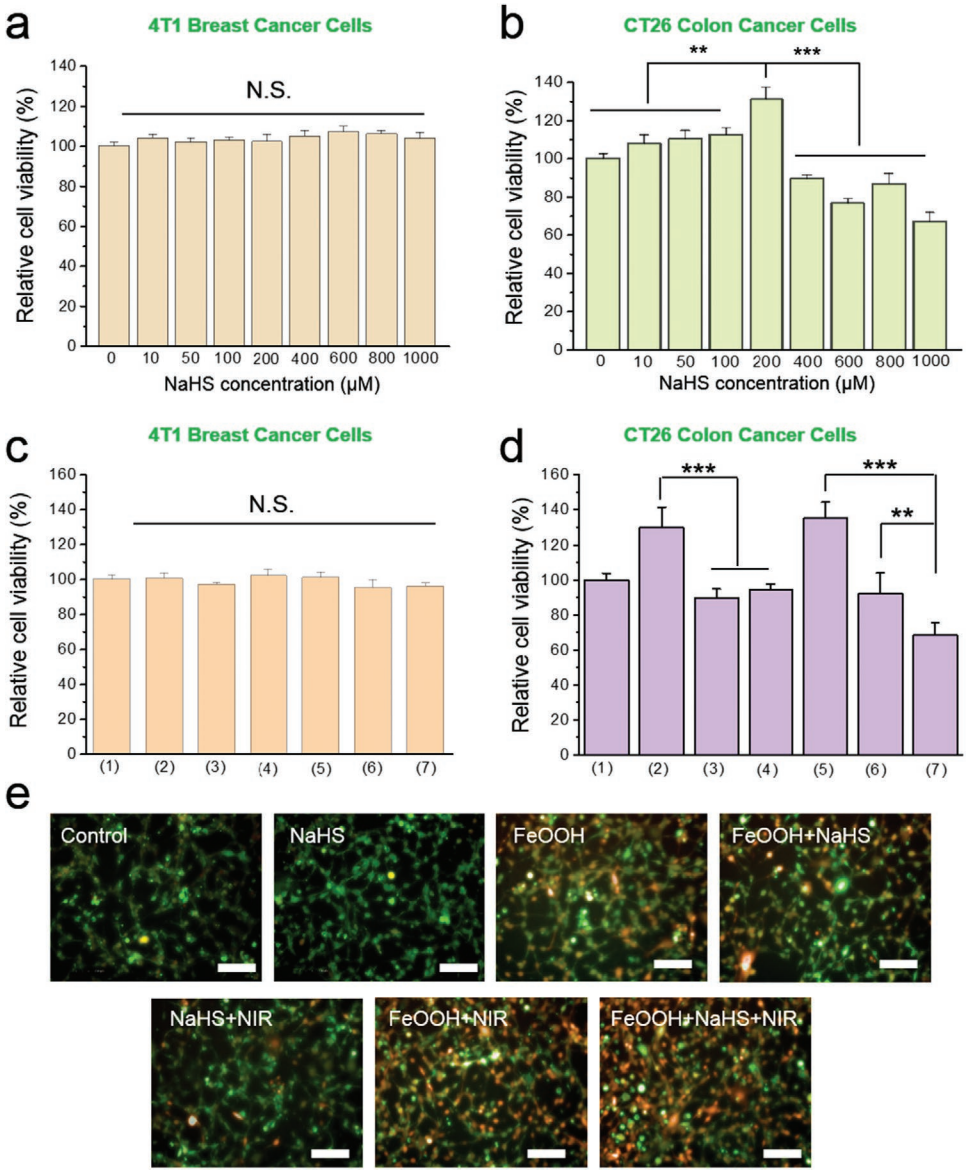

Figure 3. In vitro cell viability assay of 4T1 cells and CT26 cells. a,b) Relative cell viability of 4T1 cells and CT26 cells after 24 h of the incubation of NaHS at a series of concentrations (0–1000 × 10^{-6} M). c,d) The cell viability of 4T1 and CT26 cells with different treatments: 1) PBS; 2) NaHS; 3) FeOOH; 4) NaHS+FeOOH; 5) NaHS+NIR; 6) FeOOH +NIR; 7) NaHS+FeOOH +NIR. The cell treatment groups were irradiated by 808 nm NIR laser for 5 min and the irradiation density is 1.5 W cm^{-2}. The concentrations of all NaHS-treated groups were set at 200 × 10^{-6} M. e) Fluorescence images of CT26 cells stained with the live/dead kit after various treatments (Bar = 50 μm). The used concentration of FeOOH and NaHS is 600 × 10^{-6} and 200 × 10^{-6} M, respectively. N.S.: no significant differences; ** $p < 0.01$; *** $p < 0.001$.

fluorescence emitting from FOOH/IR780 is evenly distributed within the cytoplasm region and around the nucleus (Figure S6, Supporting Information). The results demonstrate that the FeOOH can be internalized by cancer cells to realize the therapeutic effect. Subsequently, to further confirm the smartly photothermal effect, FeOOH NSs were incubated with 4T1 and CT26 cells for identifying the H_2S-activated cytotoxicity. As can be seen in **Figure 3**a, the increasing concentration of NaHS did not induce any effects on the viability of 4T1. Although the intensive concentration of NaHS eventually caused cytotoxicity on CT26 cells, certain concentrations (up to 200 × 10^{-6} M) well boosted the cell proliferation, showing the vital role of H_2S in for colon cancer (Figure 3b). Rare cytotoxicity of FeOOH has been observed on both 4T1 and CT26 cells, showing the high biocompatibility (Figure 3c,d). In Figure 3d, the viability of CT26 cells with different treatments was conducted. The CT26 cell viability after FeOOH treatment is close to 90%, indicating the relatively low toxicity. Meanwhile, the cell viability of NaHS and NaHS+NIR treated groups is around ≈130%, suggesting the promoted growth of CT26 cell. In contrast, the incubation of FeOOH NSs effectively prevented CT26 cells from the boost effect induced by H_2S (dragging the viability from ≈130% back to ≈90%). With the "turn-on" PTT function, the cell viability of NaHS+FeOOH +NIR group is ≈68% compared with that

of CT26 after the H_2S boost (Figure 3d,e). The significantly reduced cell activity was attributed to the H_2S consumption ability and activated photothermal performance. Crucially, these H_2S triggered effects have not been observed in 4T1 breast cancer cells, clearly proving FeOOH NSs' accuracy of selectivity (Figure 3).

2.4. Effective H_2S Scavenge and Ferroptosis Induced by FeOOH NSs

A series of novel H_2S-triggered nanomedicines have been investigated for treating colon cancer by combining various imaging (photoacoustic, MRI, NIR imaging, etc.) and therapeutic modules (photodynamic and photothermal therapy, etc.),[10] few paid attention to inhibit the tumor cells by removing endogenous H_2S. Given the vital role of H_2S in colon cancer development, the feature of FeOOH NSs in H_2S scavenge was systemically examined. The increasing concentration of FeOOH NSs could greatly consume the dissolved H_2S within 1 d, with around ≈50% and ≈0% left at a concentration of 22.6 and 180.8 μg mL^{-1}, respectively (**Figure 4**a). Although the presentation of fetal bovine serum (FBS) (that might attach on the surface of NSs) affected the adsorbing capability of FeOOH NSs, most of H_2S were adsorbed within 20 h (Figure 4b). It can be clearly seen that the attendance of FeOOH NSs was able to remove all the absorbed H_2S (≈80×10^{-6} M) from CT26 cells when the concentration reached 56.5 μg mL^{-1} (Figure 4c). Notably, the further addition of FeOOH NSs could completely wipe H_2S out from CT26 cells. In comparison, only a few added H_2S was internalized by 4T1 cells, further indicating rare effects of H_2S on 4T1 cells (Figure S7, Supporting Information). The H_2S content in 4T1, CT26 cells, and FeOOH treated cells were further determined. It can be clearly seen that dissolved H_2S concentrations

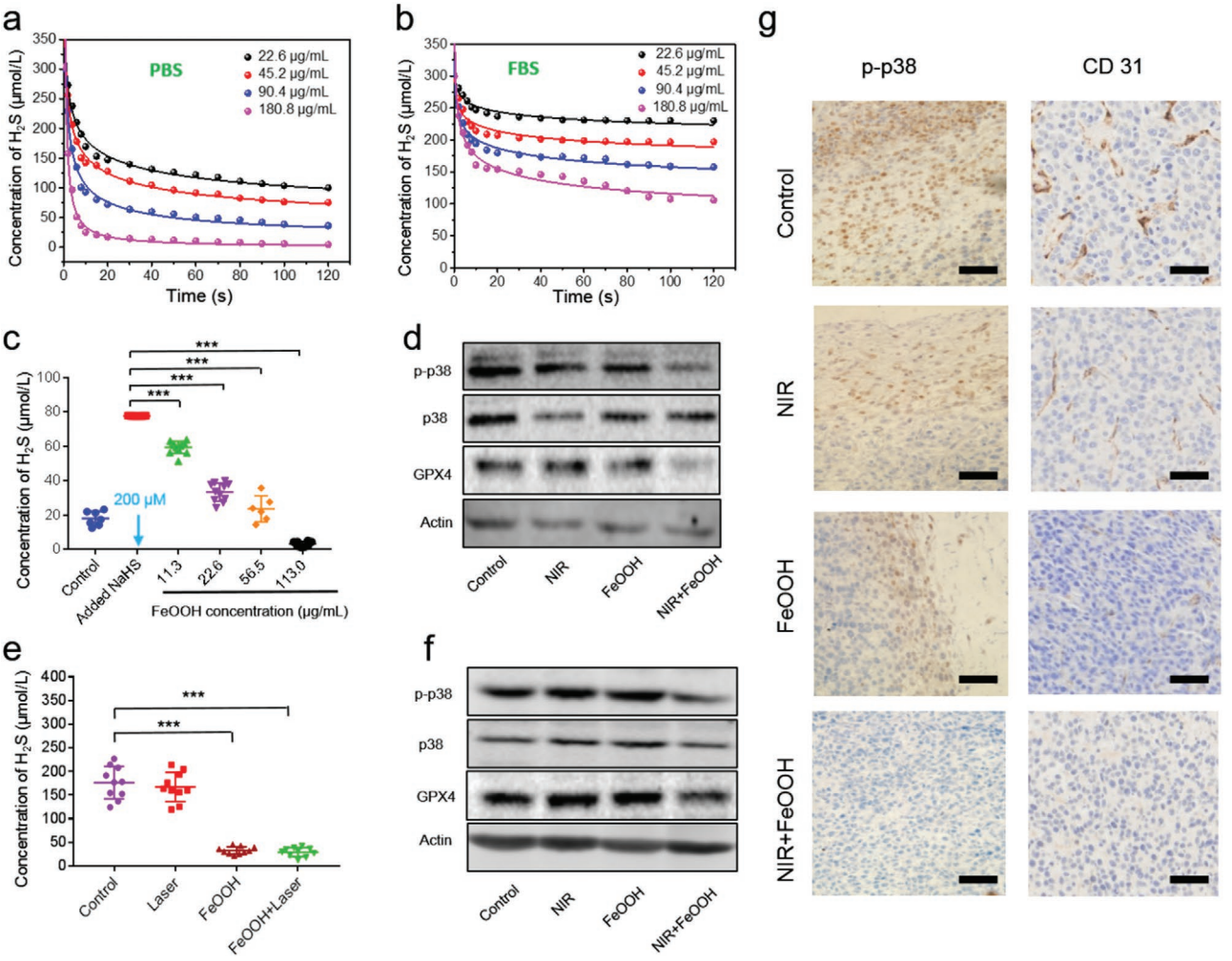

Figure 4. The in vitro and in vivo performance of FeOOH NSs in consuming H_2S. a,b) The concentration changes of dissolved hydrogen sulfide in PBS and serum solution over time in the presence of FeOOH NSs at different concentrations. The initially dissolved hydrogen sulfide concentrations in the two media were 300 μmol L^{-1}. c) The dissolved H_2S concentrations in CT26 cell lysis. The CT26 cell was cultured with different treatments: control, NaHS (the concentration was 200 μmol L^{-1}) without or with different concentrations of FeOOH NSs ($n = 8$). d) Western blot results of p-p38 and p38 expression level in CT26 cells after different treatments. e) Quantitative comparison of the intratumoral dissolved hydrogen sulfide levels after treatments ($n = 10$). f) Western blot results of p-p38, p38, and GPX4 expression levels within tumor tissue after various treatments. g) p-p38 and CD31 immunostaining of CT26 tumor sections after a series of treatments (Bar = 100 μm). *** $p < 0.001$.

in 4T1 were very low that can be almost negligible. After adding FeOOH NSs, the dissolved H_2S concentrations in 4T1 cell are still very low, and no changes were observed (Figure S8a, Supporting Information). However, the dissolved H_2S levels in CT26 cells are much higher than that of 4T1 cell. The addition of FeOOH NSs was able to effectively remove the dissolved H_2S from CT26 cells (Figure S8b, Supporting Information). The efficiency of H_2S scavenge was investigated in CT26 tumors from mice after treatments as well. The administration of FeOOH NSs significantly consumed more than 85% endogenous hydrogen sulfide within CT26 tumors, and the addition of NIR laser reached a comparable level of it (Figure 4e).

In consideration that the iron-based nanospindles could further lead to the death of tumor cells via the ferroptosis, this potential mechanism was analyzed as well.[19] In addition, we also investigated the P38 MAPK signaling pathway, which has been shown to be activated by H_2S stimulation. As shown in Figure 4d, the incubation of FeOOH NSs was able to reduce the phosphorylation of p-p38 protein in CT26 cells, while the p38 was slightly affected within the tumor (Figure 4d,f and Figure S9, Supporting Information). Apparently, the combined treatment of FeOOH NSs and NIR greatly blocked the phosphorylation of p38 protein and expression of glutathione peroxidase 4 (GPX4) simultaneously, indicating the induced ferroptosis within malignant cells and tissues (Figure 4d,f and Figure S9, Supporting Information). More specifically, IHC staining results also demonstrated that the expression of p-p38 and CD31 was obviously decreased after FeOOH NSs plus NIR treatment (Figure 4g). Consistently, the reversely decreasing levels of vessels further confirmed this trend of ferroptosis among various groups. As an important factor, the expression of p38 and GPX4 would potentially induce and inhibit the ferroptosis via the pathway of mitogen-activated protein kinases (MAPKs) and ROS generation, respectively.[24] Thus, the decreased levels of p-p38 (the increasing level of p-38) and GPX4 would promote the cancer therapeutic effect of FeOOH NSs via the ferroptosis.[25] A multiple functional nanoplatform with the high performance of H_2S scavenge, H_2S-mediated PTT, and ferroptosis could be achieved via current FeOOH NSs.

2.5. Fluorescence and MRI Imaging of FeOOH NSs

Due to the fast growth and proliferation of cancer cells, the microenvironment within the tumor area is greatly different from normal tissues, which allows advanced agents such as nanomedicines to selectively accumulate in malignant regions via enhanced permeability and retention (EPR) effect.[26] Based on our previous studies,[27] the FeOOH NSs were labeled with IR780 to investigate the biodistribution at different time points after i.v. injection. As shown in Figure S10a (Supporting Information), the FeOOH/IR780 NSs quickly accumulated in the tumor area 2 h postinjection and lasted for the following 48 h. Although the IR780 passively migrated to the tumor site within 2 h, the clearance of IR780 alone was much quicker than that was carried by FeOOH NSs, and most of the injection dose was eliminated after 24 h. Furthermore, the data of ex vivo biodistribution were consistent with NIR imaging by showing higher tumor uptake of FeOOH/IR780 NSs compared with IR780 only (Figure S10b,c, Supporting Information). These results well indicated the high efficiency of FeOOH NSs in targeting tumors. Among all the imaging modules, the MRI provides a noninvasive and precision imaging that greatly helps the preoperative diagnosis. With efficient magneto-responsive capabilities, iron-based nanospindles have been widely recruited as MRI contrast agents in preclinical and clinical applications, such as ferumoxytol.[28]

As can be seen in Figure 6a, the transverse relativity values of FeOOH NSs gradually decreased with the increasing concentration, which well proved the potential of FeOOH NSs as MRI contract agent (**Figure 5**a,b), which is consistent with reported results.[11,29] More importantly, the T_2 MRI intensity quickly reached the bottom when the concentration was above 25 μg mL^{-1}, indicating the effective T_2 MRI of FeOOH NSs. FeOOH NSs also showed a smooth field-dependent magnetization curve without any hysteresis and presented a magnetization saturation (M_S) value at 0.04 emu g^{-1} (Figure 5c). As shown in Figure 5d, the T_2 intensity within the tumor area kept decreasing even at 2 d after intravenous administration, clearly showing the accumulation of FeOOH NSs. The high-resolution TEM images and Prussian blue staining of tumor sections further confirmed the existence of iron nanospindles within the tumor area (Figure 5e,f).

2.6. Antitumor Effect of FeOOH NSs via H_2S-Activated PTT and Gas Scavenging

In comparison with other types of cancer, the progress of colorectal malignant tissues is strongly associated with hydrogen sulfide,[7a] giving a possibility for precision therapy for colon cancer. Notably, due to the toxicity, endogenous H_2S has extremely fast catabolism,[30] which relatively enhances its specificity within the colorectal tumor area compared with normal tissues. Given that, the H_2S-targeting strategy would provide better therapy than other general TME factors such as acidic pH in treating colon cancer. With promising outcomes above, the H_2S-based therapeutic effects of FeOOH NSs were further evaluated in xenograft mice models (**Figures 6** and **7**). Apparently, treatments of FeOOH NSs or FeOOH NSs plus NIR could not inhibit the growth of 4T1 tumors in terms of tumor volume, size, and weight (Figure 6a–c). Due to silenced functions of FeOOH NSs in treating breast cancer, intact tissue structure, massive blood vessels, and rare apoptosis were clearly observed within 4T1 tumors as well. Further, the CT26 tumor-bearing mice administrated with FeOOH NSs exhibited a quick increase of temperature in the tumor region and it reached to ≈59 °C within 5 min under the NIR laser irradiation. In contrast, the control group (PBS) presented a weak increase in temperature after 5 min irradiation and the temperature increment of direct NIR irradiation without FeOOH NSs was less than 5 °C (Figure S11, Supporting Information). The FeOOH NSs demonstrated the H_2S-activated photothermal performance in CT26 tumor model. The administrated FeOOH NSs efficiently scavenged the endogenous H_2S and eventually reduced the CT26 relative tumor volume from ≈67 ± 16.2 to ≈21.1 ± 8.2, while the attendance of NIR further decreased the volume to ≈14 ± 4.6 by cooperating with

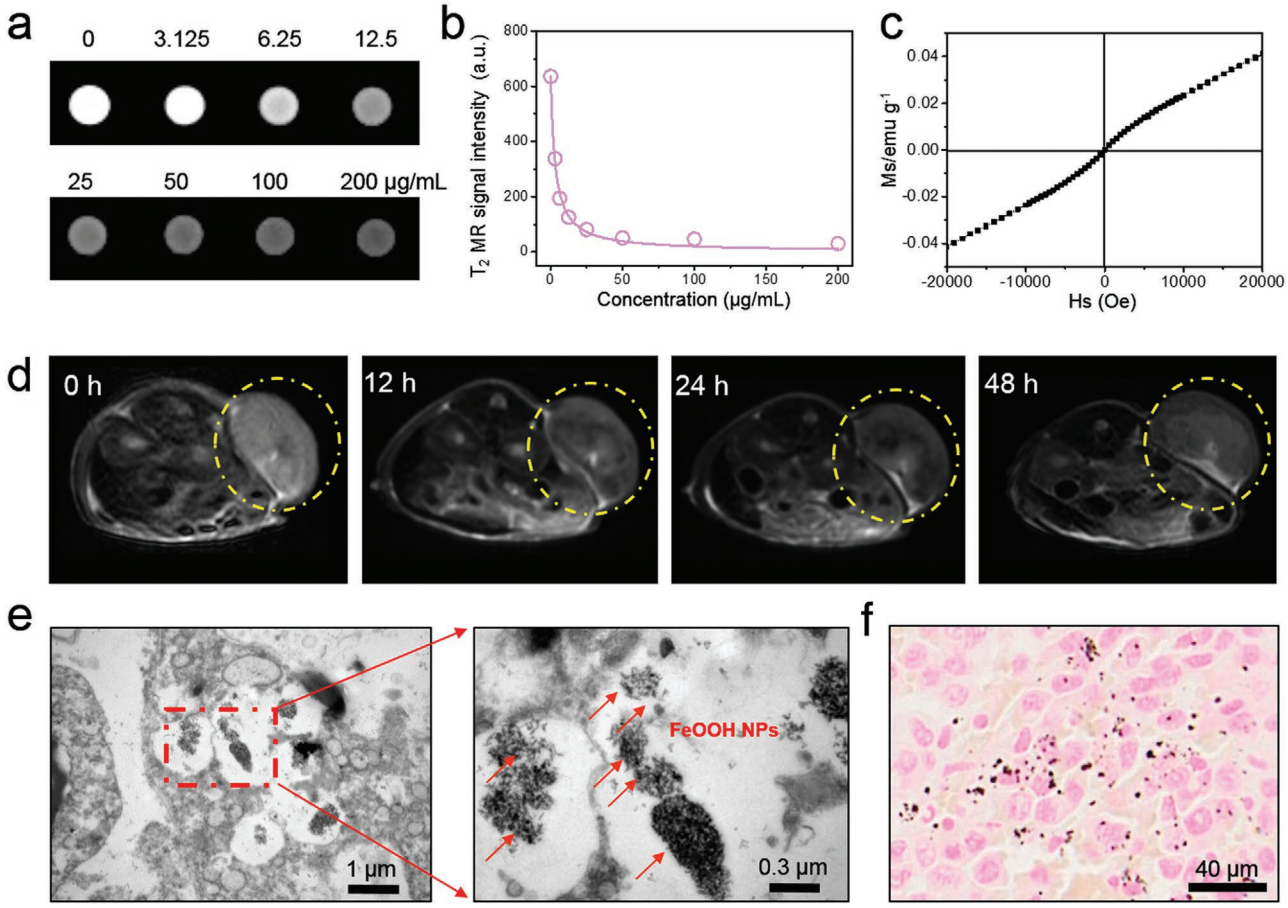

Figure 5. The evaluation of FeOOH NSs as an efficient T_2-MRI contrast agent. a,b) T_2-MRI imaging of FeOOH NSs at concentrations from 0 to 200 μg mL^{-1} and corresponding quantification. c) Field-dependent magnetization curve of FeOOH NSs measured at room temperature. d) In vivo T_2-MRI imaging of CT26-bearing mice after i.v. injection of FeOOH NSs (200 μL, 3.0 mg mL^{-1}) at different time points (0, 12, 24, and 48 h postinjection) (yellow circles point to the tumor sites). e) The TEM images of CT26 tumor sections after the treatment of FeOOH NSs. The arrows indicate FeOOH NSs. f) Histological analysis of tumor tissues with Prussian blue staining.

H_2S-activated PTT (Figure 7a). Similarly, the size and weight of CT26 tumors from mice treated with NIR-plus FeOOH NSs were smallest among all (408 mm^3 and 0.25 ± 0.15 g), which were about six times less than those of control group (≈1940 mm^3 and 1.5 ± 0.51 g) (Figure 7b,c,e). Meanwhile, the administration of FeOOH NSs also limited the growth of CT26 tumors by shrinking the sizes and weights to ≈592 mm^3 and 0.63 ± 0.12 g. Inconsistent, it can be seen in Figure 7f that much loose and irregular cell morphology could be identified within the CT26 tumor after FeOOH NSs and NIR treatment, followed by that from FeOOH NSs group. Obviously, compared to control, NIR, and FeOOH groups, CT26 tumors in the FeOOH+NIR group demonstrated higher TUNEL apoptotic signals, fewer percentage of Ki67 expression and HSP70 cells. Notably, the treatments did not cause any side effects on either mice bearing 4T1 and CT26 tumors in terms of body weight and major organs (Figures 6d and 7d,h). To date, several H_2S-activated nanoplatforms have been successfully applied in colon cancer treatment, most of them (except of Cu_2O nanospindles) have to be administrated locally (intratumor or subcutaneous injection).[16,31] Furthermore, the single therapeutic module (e.g., PTT or PA only) and potential side effect (e.g., toxicity) might limit the outcome of treatment.[27] In comparison, the desirable stability and multiple functions including H_2S removal, H_2S-triggered PTT and ferroptosis provided by FeOOH NSs would greatly promote and ensure the therapeutic outcome via various effects. Besides, the high tumor specificity by H_2S-triggered PTT would efficiently avoid the damage on normal tissues from the off-target effect.

2.7. The Desirable Biosafety of FeOOH NSs

For any clinical translation, the biosafety is of vital importance in quality control. In this work, the in vitro toxicity of FeOOH nanoparticles has been investigated in two kinds of normal cells. As demonstrated in Figure S12 (Supporting Information), the relative viabilities of human embryonic kidney 293 and hepatocyte-derived liver cells were above ≈80% with the concentration from 0 to 9600 × 10^{-6} M for 24 h. Although the cytotoxicity of FeOOH NSs was hardly detected from the histological assays, the potential side effects could not be ignored before its real application in the clinic. Thus, a series of histological, blood biochemistry, and hematologic biosafety studies

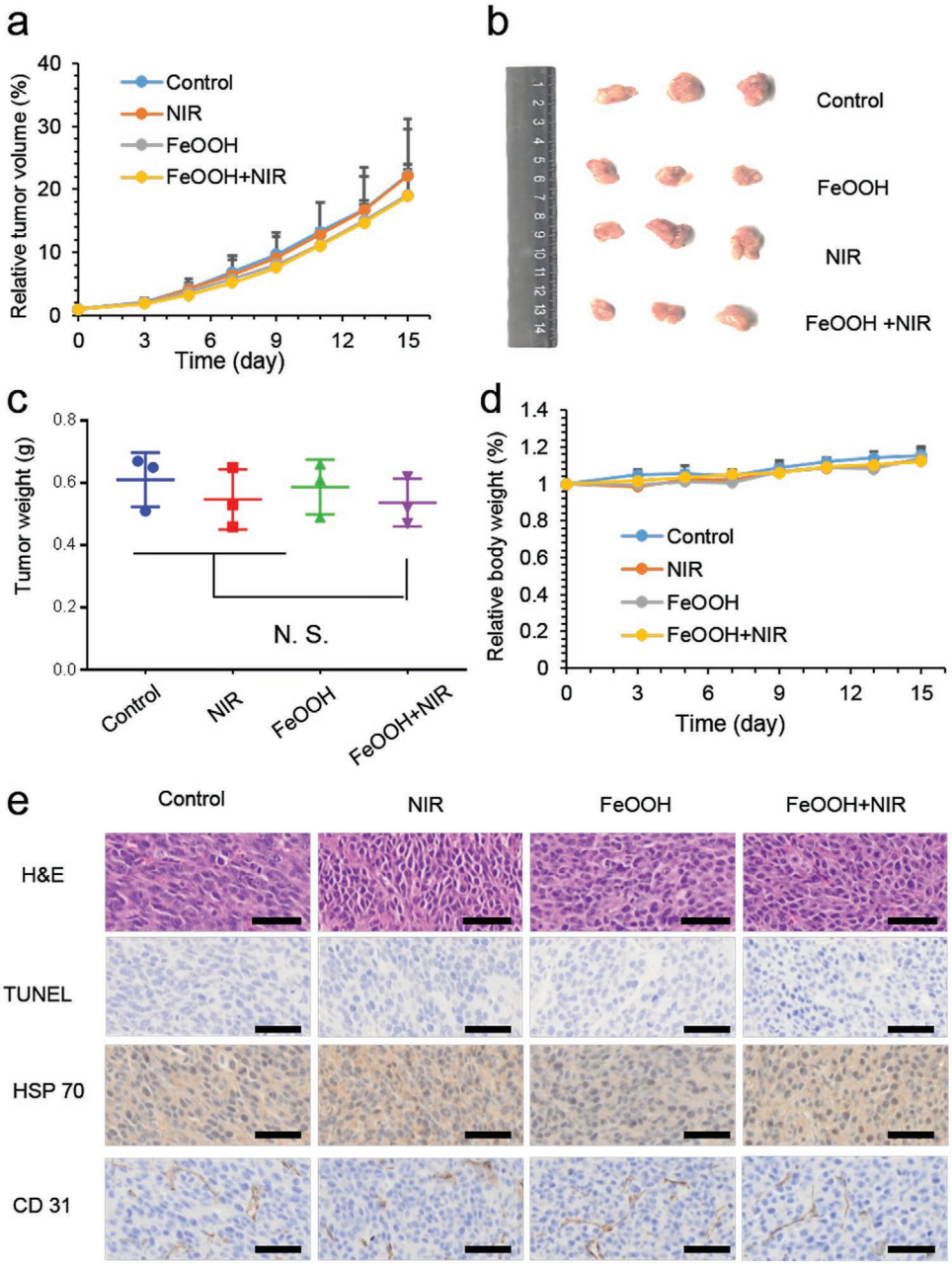

Figure 6. Evaluation of the therapeutic effect of FeOOH NSs in 4T1 breast tumor-bearing mice. a) The trends of relative tumor volume of different groups over time (from 0 to 15 d). b) Optical photograph of excised tumors from the mice after different treatments at 15 d. c) Quantification of tumor weight at 15 d after the treatments. d) The curves of relative body weight during the therapy. e) The H&E, TUNEL, HSP70, and CD31 immunostaining of tumor sections from different groups. Bar = 50 μm.

were conducted for evaluating the biosafety of FeOOH NSs. To comprehensively monitor and investigate the potential cytotoxicity, all the assays were last for three months. Obviously, the administration of FeOOH NSs did not cause any morphological changes in major organs for 90 d (**Figure 8**a). Additionally, there was not any difference between mice treated and untreated with FeOOH NSs in terms of body weight (Figure 8b). Importantly, the blood biochemistry (e.g., ALT, AST, etc.) and hematologic (e.g., WBC, RBC, etc.) examinations clearly indicated the desirable biosafety of FeOOH NSs (Figure 8c–n).

3. Conclusion

In summary, we have successfully developed a novel H_2S-responsive FeOOH NSs for the colon cancer combination therapy, specifically. The as-prepared FeOOH NSs can scavenge H_2S in vitro and in vivo efficiently. The particular H_2S-driven reduction reaction produced FeS demonstrated a strong NIR absorption and good photothermal performance. Moreover, the inactivation of GPX4 caused by Fe^{2+}-mediated ferroptosis direct tumor cell death. Meanwhile, this H_2S-activated

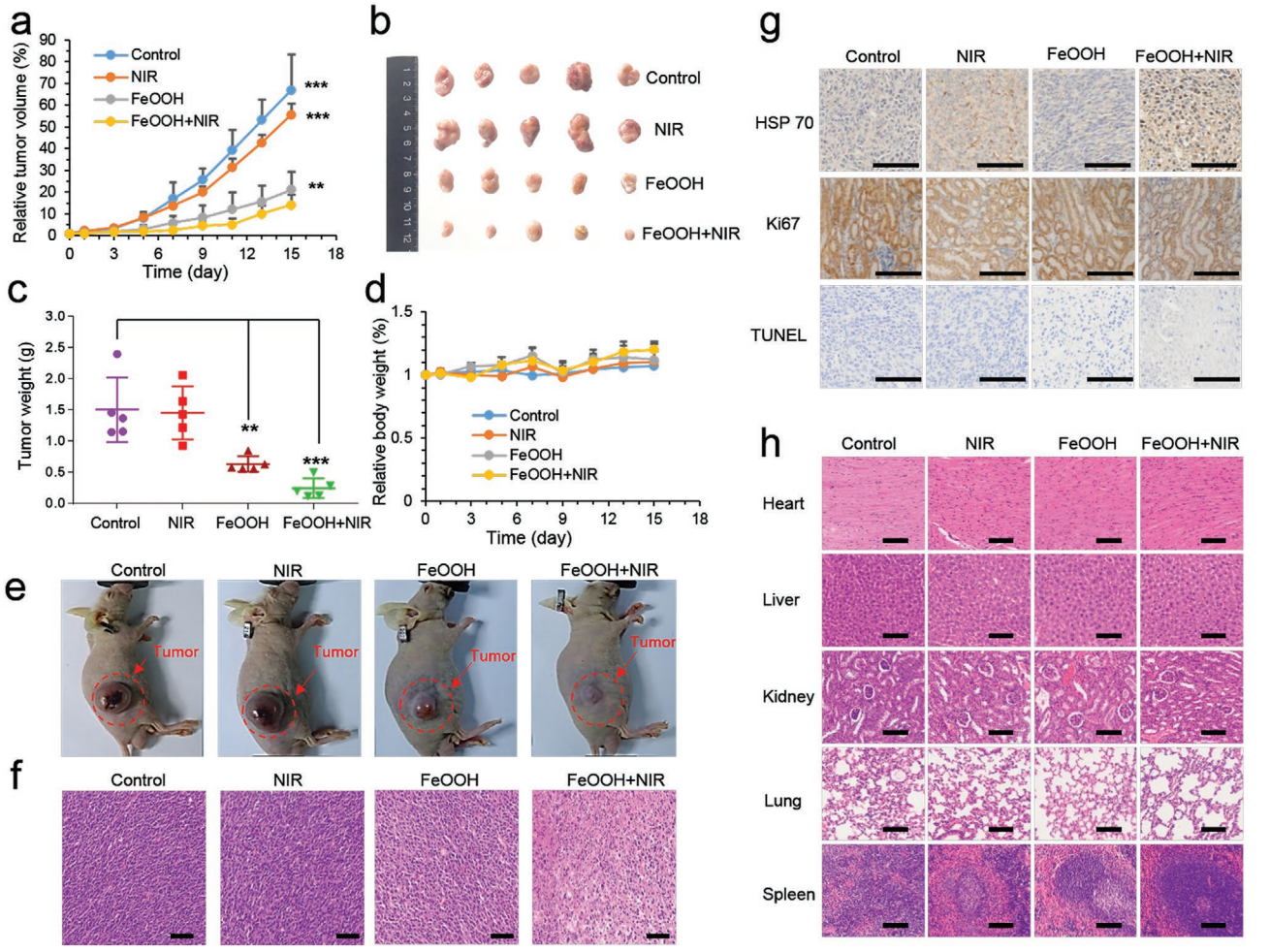

Figure 7. The therapeutic performance of FeOOH NSs in treating CT26 colon tumors. a) The growing curves of relative tumor volume among different groups from 0 to 15 d. b) Optical images of the excised tumors from mice at 15 d post various treatments. c) The tumor weights at 15 d after the treatments. d) The relative bodyweight curves throughout the treatments. e) Optical photographs of tumor-bearing mice from different groups after 15 d treatments and f) tumor sections stained with H&E. g) The representative HSP70, Ki-67, and TUNEL immunohistochemical staining of tumor tissues from different groups at day 15, Bar = 100 μm. h) The hematoxylin and eosin staining of major organs (heart, liver, kidney, lung, and spleen) from mice at 15 d post treatments. Bar = 100 μm.

nanotheranostics induced a negligible cure effect in 4T1 breast cancer. Additionally, these multifunctional FeOOH NSs were able to detect tumors as an effective MRI contrast agent, and no long-term toxicity was detected in the murine model for up to three months. All these findings clearly indicate that the multifunctional FeOOH NS is a powerful platform for colon cancer theranostics, holding great potential for future clinical translation.

4. Experimental Section

Synthesis of FeOOH NSs: FeOOH NSs were prepared via a simple and homogeneous precipitation method according to previous studies.[20] Briefly, $FeCl_3{\cdot}6H_2O$ (0.5 M, 10 mL) was first mixed with HCl (0.04 M, 10 mL), then mixed with dopamine hydrochloride solution (1.6 mg mL^{-1}, 10 mL) under stirring for 5 min. Subsequently, 180 mL of water (90 °C) was added and stirred for another 2 h. After cooling to room temperature, the NaOH solution (1 M, 3 mL) was slowly dropped into the mixture until the precipitation of FeOOH NSs appeared. Subsequently, the FeOOH NSs samples were collected by centrifuge at 12 000 rpm. Finally, FeOOH NSs were dispersed in aqueous solution for further surface modification.

Subsequently, PEG modification process was further conducted. First, 10 mL of a polyacrylic acid (PAA) solution (MW = 1800, 1 mg mL^{-1}) was added to the FeOOH NSs solution under stirring for 6 h at room temperature. FeOOH-PAA solution was obtained and washed with deionized water to remove free PAA molecules. Subsequently, 10 mL PEG-NH_2 (Mw = 5 kDa) solution at the concentration of 10 mg mL^{-1} was added into the FeOOH-PAA solution, stirring for 1 h. Then, 200 mg N-(3-dimethylaminopropyl-N′-ethylcarbodiimide) hydrochloride (EDC) was added into the mixture and stirred overnight. Finally, PEGylated FeOOH NSs were harvested through centrifugation and washed twice with deionized water. The obtained PEGylated FeOOH NSs were stored at 4 °C for further use.

In Vitro Biocompatibility and H_2S-Mediated Cytotoxicity FeOOH NSs: 4T1 cells and CT26 cells were maintained in DMEM (10%) supplemented with 1% antibiotics (100 U mL^{-1} penicillin and 100 μg mL^{-1} streptomycin) at 37 °C in a 5% CO_2 atmosphere. 4T1 cells and CT26 cells were first seeded in 96-well plate at 5 × 10^3 cells per well for 24 h; then FeOOH NSs were incubated with cells for another 24 h. PTT was performed by irradiating cells with an 808-nm laser (MDL-N-808-10W, Changchun, China). The irradiation density was 1.5 W cm^{-2}, while the irradiation time was 5 min.

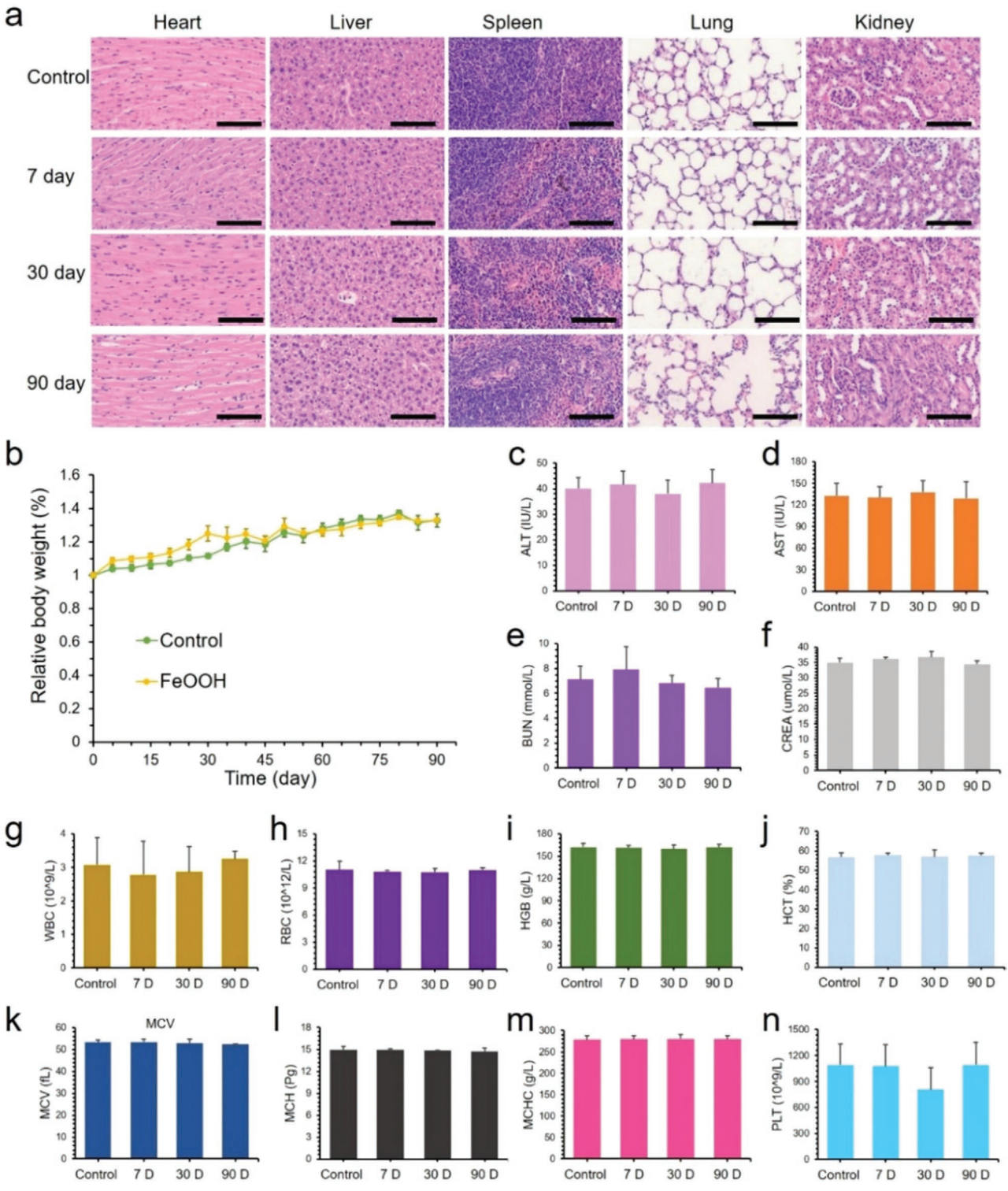

Figure 8. Preliminary biosafety evaluation of FeOOH NSs in the murine model. a) H&E staining of major organs from healthy mice and mice after i.v. injection of FeOOH NSs (Bar = 100 μm). b) The variation of body weight between the two groups. c–n) The blood biochemistry and hematology assays of normal mice treated with FeOOH NSs at a dose of 5 mg mL^{-1} (200 μL) at 1, 15, and 30 d p.i. The testing parameters included examinations of aminotransferase (ALT), aminotransferase (AST), blood urea nitrogen (BUN), creatinine (CREA), white blood cell (WBC) counts, red blood cell (RBC) counts, hemoglobin (HGB), hematocrit (HCT), mean corpuscular volume (MCV), mean corpuscular hemoglobin (MCH), mean corpuscular hemoglobin concentration (MCHC), and platelets (PLT).

Then, the cell viability was measured by using the 3-(4, 5-dimethylthiazol-2-yl)-2, 5-diphenyltetrazolium bromide (MTT) assay kit (YEASEN, Shanghai, China). Meanwhile, the live/dead cells were detected by using a Calcein-AM/PI double stain kit (YEASEN, Shanghai, China), and imaged on a high intension cell imaging analysis system (PerkinElmer, USA).

Hydrogen Sulfide Consumption via FeOOH NSs: NaHS was used to simulate endogenous H_2S for investigating the H_2S consumption mediated by FeOOH NSs. NaHS was dissolved in different solution media (PBS and FBS medium) to simulate the dissolved hydrogen sulfide. Then, the same volume FeOOH NSs solution with different concentrations was added into the solution for 2 h. The dissolved hydrogen sulfide concentration was measured by using an Unisense hydrogen sulfide microelectrode as a function of time.

Endogenous hydrogen sulfide in colon cancer cells (CT26 cells) was measured via similar methods. Briefly, CT26 cells were first seeded and cultured overnight with complete medium with 10% FBS and 1% penicillin/streptomycin at 37 °C under 5% CO_2. The culture media were then replaced by fresh media with the following substances: PBS, NaHS (200×10^{-6} M), and NaHS (200×10^{-6} M) plus different concentrations of FeOOH NSs. After a further incubation at 37 °C in 5% CO_2 for 24 h, cells were collected and washed with PBS for three times. Then, the cells from all groups were dispersed in PBS solution and then broken by an ultrasonic cell grinder. The dissolved hydrogen sulfide concentration was measured by the same Unisense oxygen microelectrode. Endogenous hydrogen sulfide in 4T1 cells was measured via the same methods. The endogenous H_2S within CT26 tumor was further analyzed as well. Briefly, mice bearing CT26 tumors were i.v. injection of FeOOH NSs at the concentration of 3 mg mL^{-1} (in terms of Fe). Then, CT26 tumors were harvested and lysed. The supernatant was obtained after centrifugation and measured for the dissolved hydrogen sulfide concentration on an Unisense hydrogen sulfide microelectrode.

Therapeutic Effects of FeOOH NSs in Mice Bearing 4T1 and CT26 Tumors: All animal experiments were approved by the Institutional Animal Care and Use Committee of Zhejiang University School of Medicine. The antitumor study was carried in both 4T1 and CT26 tumor-bearing nude mice. When sizes of tumors reached about 30 mm^3, mice were randomly divided into four groups ($n = 5$): control, NIR (laser), FeOOH, and FeOOH+NIR laser. Mice bearing 4T1 or CT26 tumors were i.v. injected with FeOOH (3 mg mL^{-1} [Fe]). Mice from NIR and FeOOH+NIR groups were irradiated with 808 nm NIR laser at a power density of 1.5 W cm^{-2} for 5 min at 24 h postadministration. The tumor sizes were measured every 2 d and calculated according to the following formula: the tumor volume = (tumor length) × (tumor width)^2/2. The relative tumor volumes were defined as V/V_0 (V_0 is the beginning volume). After treatment, tumors from different groups were collected for hematoxylin and eosin (H&E) and immunohistochemical analysis.

Supporting Information

Supporting Information is available from the Wiley Online Library or from the author.

Acknowledgements

Y.Y.L., Y.C.Q., and W.Y.C. contributed equally to this work. This work was supported by the National Key Research and Development Program of China (No. 2018YFC0115701), the National Natural Science Foundation of China (Nos. 81671748 and 81971667), and China Postdoctoral Science Foundation (2017M620243). The authors thank the technical support by the Core Facility, Zhejiang University School of Medicine.

Conflict of Interest

The authors declare no conflict of interest.

Keywords

colon cancer, ferroptosis, hydrogen sulfide, iron oxide-hydroxide nanospindles, photothermal therapy

Received: March 2, 2020
Revised: June 6, 2020
Published online:

[1] a) A. A. Untereiner, A. Pavlidou, N. Druzhyna, A. Papapetropoulos, M. R. Hellmich, C. Szabo, *Biochem. Pharmacol.* **2018**, *149*, 174; b) I. Marmol, C. Sanchez-de-Diego, A. P. Dieste, E. Cerrada, M. J. R. Yoldi, *Int. J. Mol. Sci.* **2017**, *18*, 197.
[2] a) Y. Shaked, *Nat. Rev. Cancer* **2019**, *19*, 667; b) S. Cassidy, B. A. Syed, *Nat. Rev. Drug Discovery* **2017**, *16*, 525.
[3] M. Schünemann, S. D. Anker, M. Rauchhaus, *Nat. Clin. Pract. Oncol.* **2008**, *5*, 632.
[4] C. Holohan, S. Van Schaeybroeck, D. B. Longley, P. G. Johnston, *Nat. Rev. Cancer* **2013**, *13*, 714.
[5] R. A. Smith, V. Cokkinides, A. C. von Eschenbach, B. Levin, C. Cohen, C. D. Runowicz, S. Sener, D. Saslow, H. J. Eyre, *CA: Cancer J. Clin.* **2002**, *52*, 8.
[6] J. L. Wallace, R. Wang, *Nat. Rev. Drug Discovery* **2015**, *14*, 329.
[7] a) C. Szabo, C. Coletta, C. Chao, K. Módis, B. Szczesny, A. Papapetropoulos, M. R. Hellmich, *Proc. Natl. Acad. Sci. USA* **2013**, *110*, 12474; b) W. J. Cai, M. J. Wang, L. H. Ju, C. Wang, Y. C. Zhu, *Cell Biol. Int.* **2010**, *34*, 565; c) M. Wang, J. Yan, X. Cao, P. Hua, Z. Li, *Biochem. Pharmacol.* **2020**, *172*, 113775.
[8] C. Szabo, *Nat. Rev. Drug Discovery* **2016**, *15*, 185.
[9] C. Tao, L. An, J. Lin, Q. Tian, S. Yang, *Small* **2019**, *15*, 1903473
[10] W. Chen, D. Ni, Z. T. Rosenkrans, T. Cao, W. Cai, *Adv. Sci.* **2019**, *6*, 1901724.
[11] a) M. Kumagai, Y. Imai, T. Nakamura, Y. Yamasaki, M. Sekino, S. Ueno, K. Hanaoka, K. Kikuchi, T. Nagano, E. Kaneko, *Colloids Surf., B* **2007**, *56*, 174; b) M. L. Chen, L. M. Shen, S. Chen, H. Wang, X. W. Chen, J. H. Wang, *J. Mater. Chem. B* **2013**, *1*, 2852; c) L. Zeng, W. Ren, J. Zheng, A. Wu, P. Cui, *Appl. Surf. Sci.* **2012**, *258*, 2570.
[12] S. Lee, T. Lee, D. Kim, *Ind. Eng. Chem. Res.* **2017**, *56*, 3116.
[13] a) L. Cheng, J. Liu, X. Gu, H. Gong, X. Shi, T. Liu, C. Wang, X. Wang, G. Liu, H. Xing, W. Bu, B. Sun, Z. Liu, *Adv. Mater.* **2014**, *26*, 1886; b) M. Wen, S. Wang, R. Jiang, Y. Wang, Z. Wang, W. Yu, P. Geng, J. Xia, M. Li, Z. Chen, *Biomater. Sci.* **2019**, *7*, 4651; c) X. Zhao, C. X. Yang, L. G. Chen, X. P. Yan, *Nat. Commun.* **2017**, *8*, 14998.
[14] a) Y. Liu, P. Bhattarai, Z. Dai, X. Chen, *Chem. Soc. Rev.* **2019**, *48*, 2053; b) X. Zhu, J. Li, X. Qiu, Y. Liu, W. Feng, F. Li, *Nat. Commun.* **2018**, *9*, 2176.
[15] Y. T. Li, J. L. Zhou, L. Wang, Z. G. Xie, *ACS Appl. Mater. Interfaces* **2020**, *12*, 30213.
[16] L. An, X. Wang, X. Rui, J. Lin, H. Yang, Q. Tian, C. Tao, S. Yang, *Angew. Chem., Int. Ed.* **2018**, *57*, 15782.
[17] C. H. Zhang, Y. Wang, Q. Q. Sun, L. L. Xia, J. J. Hu, K. Cheng, X. Wang, X. X. Fu, H. Gu, *Int. J. Biol. Sci.* **2018**, *14*, 1834.
[18] K. Yang, G. Yang, L. Chen, L. Cheng, L. Wang, C. Ge, Z. Liu, *Biomaterials* **2015**, *38*, 1.
[19] a) A. Tarangelo, S. J. Dixon, *Nat. Nanotechnol.* **2016**, *11*, 921; b) S. Zanganeh, G. Hutter, R. Spitler, O. Lenkov, M. Mahmoudi, A. Shaw, J. S. Pajarinen, H. Nejadnik, S. Goodman, M. Moseley, *Nat. Nanotechnol.* **2016**, *11*, 986.
[20] M. Tadic, I. Milosevic, S. Kralj, M. Mitric, D. Makovec, M. L. Saboungi, L. Motte, *Nanoscale* **2017**, *9*, 10579.
[21] Y. Piao, J. Kim, H. B. Na, D. Kim, J. S. Baek, M. K. Ko, J. H. Lee, M. Shokouhimehr, T. Hyeon, *Nat. Mater.* **2008**, *7*, 242.

[22] H. Otsuka, Y. Nagasaki, K. Kataoka, *Adv. Drug Delivery Rev.* **2003**, *55*, 403.
[23] Y. Zhang, X. Zhan, J. Xiong, S. Peng, W. Huang, R. Joshi, Y. Cai, Y. Liu, R. Li, K. Yuan, *Sci. Rep.* **2018**, *8*, 8720.
[24] a) Y. Xie, W. Hou, X. Song, Y. Yu, J. Huang, X. Sun, R. Kang, D. Tang, *Cell Death Differ.* **2016**, *23*, 369; b) Y. Yu, Y. Xie, L. Cao, L. Yang, M. Yang, M. T. Lotze, H. J. Zeh, R. Kang, D. Tang, *Mol. Cell. Oncol.* **2015**, *2*, e1054549.
[25] W. Bao, X. Liu, Y. Lv, G. H. Lu, F. Li, F. Zhang, B. Liu, D. Li, W. Wei, Y. Li, *ACS Nano* **2019**, *13*, 260.
[26] S. K. Golombek, J. N. May, B. Theek, L. Appold, N. Drude, F. Kiessling, T. Lammers, *Adv. Drug Delivery Rev.* **2018**, *130*, 17.
[27] a) Y. Y. Li, Y. C. Qi, H. B. Zhang, Z. M. Xia, T. T. Xie, W. L. Li, D. N. Zhong, H. L. Zhu, M. Zhou, *Biomaterials* **2020**, *226*, 119538; b) F. Z. Dahmani, D. N. Zhong, Y. C. Qi, A. E. G. Dahmani, T. T. Xie, B. Zhou, W. L. Li, K. Yao, L. Li, M. Zhou, *J. Mater. Chem. B* **2019**, *7*, 4484.
[28] H. Wei, O. T. Bruns, M. G. Kaul, E. C. Hansen, M. Barch, A. Wiśniowska, O. Chen, Y. Chen, N. Li, S. Okada, *Proc. Natl. Acad. Sci. USA* **2017**, *114*, 2325.
[29] D. N. Zhong, J. Zhao, Y. Y. Li, Y. Qiao, Q. Wei, J. He, T. T. Xie, W. L. Li, M. Zhou, *Biomaterials* **2019**, *219*, 119369.
[30] V. Vitvitsky, O. Kabil, R. Banerjee, *Antioxid. Redox Signaling* **2012**, *17*, 22.
[31] a) Y. Ma, X. Li, A. Li, P. Yang, C. Zhang, B. Tang, *Angew. Chem., Int. Ed.* **2017**, *56*, 13752; b) B. Shi, Q. Yan, J. Tang, K. Xin, J. Zhang, Y. Zhu, G. Xu, R. Wang, J. Chen, W. Gao, *Nano Lett.* **2018**, *18*, 6411.